Features of the Band Structure and the Mechanism of Lateral Photoconductivity in Hybrid Structures T/SiO$_2$/Si (T = Fe, Fe$_3$O$_4$, TiO$_2$)

© T.A. Pisarenko [1,2], V.V. Korobtsov [1], A.A. Dimitriev [1,2], V.V. Balashev [1,2,3], V.V. Zheleznov [4]

[1] Institute of Automation and Control Processes, Far East Branch, Russian Academy of Sciences,
Vladivostok, Russia
[2] Far Eastern Federal University,
Vladivostok, Russia
[3] V.I. Il'ichev Pacific Oceanological Institute, Far Eastern Branch, Russian Academy of Sciences,
Vladivostok, Russia
[4] Institute of Chemistry, Far East Branch, Russian Academy of Sciences,
Vladivostok, Russia

E-mail: balashev@mail.dvo.ru

This paper presents the results of studying the lateral photovoltaic effect in hybrid structures based on SiO$_2$/Si depending on the nature of the conductivity of the material of the upper layer (Fe is a metal, Fe$_3$O$_4$ is a semimetal, TiO$_2$ is a semi-insulator). It is shown that this effect is observed in hybrid structures in which a depleted region with a significant band bending is formed at the SiO$_2$/Si interface. Theoretical calculations of the lateral photovoltage based on the energy parameters of the band diagrams showed that an increase in the sensitivity of the lateral photoelectric effect is associated with an increase in the built-in potential at the SiO$_2$/Si interface. It has been established that the transient characteristics of the lateral photoelectric effect, such as the rise and fall times of the photovoltage signal, are determined by the configuration of the RC-filter in the near-contact region, which depends on the conductivity of the upper layer. It is shown that, in the case of the lateral photovoltaic effect, current transfer occurs along the inversion layer, and the upper layer serves to generate a quasi-$p-n$ junction at the SiO$_2$/Si interface.

Keywords: lateral photovoltaic effect, hybrid structures, iron, magnetite, titanium dioxide.

1. Introduction

The lateral photovoltaic effect (LPE) has been intensively studied for a long time due to its wide application in optoelectronic devices. This effect was first detected when the $p-n$-transition [1,2] was irregularly illuminated, and consists in the fact that in the illuminated area, the photo-generated electron-hole pairs diffusing to the transition are separated by its electrostatic field, the local excess concentration of non-equilibrium photo-carriers leads to their asymmetric diffusion along the transition resulting in a lateral photo-voltage (LPV), which changes linearly with changing light spot position. It is known [3], that such a transition can be created, under certain conditions, in metal−semiconductor (MS) and metal−oxide-semiconductor (MOS) structures as well. In this case, electron-hole pairs generated in the illuminated area of the semiconductor substrate and diffusing into the spatial charge area are separated by an built-in potential, locally lowering the height of the built-in barrier [4–7]. As a result of this reduction, the excess photo-generated electrons and holes move along the inversion layer and the substrate, respectively, creating a lateral photo-voltage in addition to the traditional transverse photo-voltage between the inversion layer and the substrate. For a number of years, LPE has been measured in MS and MOS

structures on the semiconductor substrate side [1,2,4,8], as the effect on the metal layer side was offset by the high conductivity [4,8]. However, in [9,10], it was found that in the case of nanometer metal films, which have high resistivity, the LPV value on the top layer side becomes larger than that on the substrate [11]. The reason for the higher LPV value is a decrease in diffusion scattering in the area of the measurement contacts due to an order of magnitude decrease in the transverse distance from the built-in barrier to the contacts. Moreover, as has been shown in [11,12], the introduction of superfine SiO$_2$ layers also improves the LPE characteristics. This improvement is due to the fact that the tunnel-thin layers of SiO$_2$ prevent the formation of buffer silicide layers at the Me/Si interface, which form at the initial stage of metal film deposition and are an additional source of scattering and „parasitic contact phenomena". Thus, tunnel-thin layers of SiO$_2$ allow to create a sharp interface with a predictable value of the built-in potential. It should be noted that most works on LPE in MOS structures propose a model of current transfer, according to which, the photo-generated carriers are separated by an built-in field and are thrown into the upper metallic layer [11,13], and the LPE theory developed earlier for $p-n$-transitions [1,2] is used to analyze the LPE characteristics. On the other hand, the authors of some

works [10,14–18] believe that the inversion layer at the SiO_2/Si interface contributes to the lateral photovoltage, assuming the photocurrent flows through the inversion layer, and the role of the metal film in this case is reduced to forming $p-n$-transition at the interface. Thus, the question about the mechanism of lateral photoconductivity remains open.

A peculiarity of the lateral photovoltage is its linear dependence on the position of the laser spot between the measuring electrodes, which allows to use LPE in such devices as position-sensitive detectors (PSD). The main performance characteristics of PSD are LPE sensitivity and non-linearity [6–8,11], and response and relaxation times of photo-voltage under pulsed illumination [18–21]. Among non-contact optical sensors, the attractiveness of LPE-based PSD is due to the absence of additional data processing, high sensitivity, and short photo-response times. As follows from the analysis of the results of numerous LPE studies [12–15,18,21], the choice of material, both the top layer and the substrate, plays an important role in pulsed illumination. However, a detailed analysis of the transient processes, taking into account the mechanisms of lateral photoconductivity, is not available in the literature.

The aim of this work was to comparatively investigate the LPE features in hybrid structures depending on the type of layer material deposited on the oxidized silicon surface. The top layer materials chosen were metal (Fe), semi-metal (Fe_3O_4) and semi-insulator (TiO_2). Magnetite (Fe_3O_4) and titanium dioxide (TiO_2) were chosen due to their high resistivity and oxidation resistance. A detailed study of LPE in $Fe/SiO_2/Si$ and $Fe_3O_4/SiO_2/Si$ structures formed on silicon substrates of both conductivity types has been done by us earlier [16,17]. It was found [17] that in the $Fe/SiO_2/Si$ structure, LPE is observed at both types of substrate conductivity, but with different sensitivity. Whereas in the $Fe_3O_4/SiO_2/Si$ structure, as shown in [16], linear LPV dependence was observed only on the n-type substrate, while on the p-type substrate, photo-voltage was observed only in the near-contact regions. To extend the conductivity range of the top layer, in this work we have added a $TiO_2/SiO_2/Si$ structure with a low-conducting TiO_2 manganese-doped layer. In the $TiO_2/SiO_2/Si$ structure, the lateral photo-voltage was also measured on both conductivity type substrates, but the studied effect was only observed in the p-Si structure. The time characteristics of $U(t)$ hybrid structures under pulsed illumination were also determined. To explain the LPE features in hybrid structures, we made theoretical calculations of energy band diagrams of investigated structures, based on which a two-channel model of lateral photoconductivity is proposed.

2. Methods of production and research of samples

The hybrid structures were grown on single-crystal Si(001) n- and p-type substrates with resistivities of 7.5 and $4.5 \, \Omega \cdot cm$ respectively. An ultrathin SiO_2 layer on the silicon surface was formed by immersing the substrate in nitric acid (68% HNO_3) at 121°C for 10 min. The SiO_2, layer thickness obtained by this method is $\sim 1.5 \, nm$ [22]. The growth of iron and magnetite films on $SiO_2/Si(001)$ substrates was carried out in an ultra-high vacuum molecular beam epitaxy chamber „Katun". Film thicknesses were measured by spectral ellipsometry and atomic-force microscopy (AFM). After loading into the vacuum chamber, the $SiO_2/Si(001)$ substrates were preheated at 500°C for 1 h. Iron films between 5 and 10 nm thick were grown at a substrate temperature of 20°C. The Fe deposition was carried out at a rate of 2.5 nm/min by thermal evaporation from the Knudsen cell. Magnetite films of 20 to 100 nm thickness were grown on $SiO_2/Si(001)$ surface by reactive Fe deposition in an O_2 atmosphere at substrate temperature 300°C and oxygen partial pressure — $3 \cdot 10^{-6}$ Torr. Manganese-doped TiO_2 modification anatase films were formed on an oxidized silicon surface *ex-situ* via a templant *sol-gel*-method [23]. The samples of different thicknesses were produced by controlled deposition, namely by incubation at 75°C for a certain time $(40-55 \, min)$ of manganese-doped titanium dioxide sol on $SiO_2/Si(001)$ surface. The weight ratio of manganese to titanium was chosen as 0.15 $(Ti_{0.85}Mn_{0.15}O_2)$. After deposition, the silicon wafers with the deposited film were annealed at 500°C for 2 h.

In order to measure the photovoltage on the surface of the films, aluminum contacts were obtained in the form of two strips of 2×1 mm, with a spacing of 2 mm between them. The contacts were obtained by thermo-vacuum spraying aluminum through a metal mask mounted on 6×4 mm samples. Illumination was provided by a He-Ne laser with $\lambda = 633 \, nm$, a beam diameter of $50 \, \mu m$ and an irradiation power incident on the sample surface of 0.3 mW. The photovoltage $U(x)$ and $U(t)$ dependences were measured using a Keithley-2000 and an AKIP-4115/5A digital oscilloscope, respectively.

3. Results and discussion

We investigated the LPE in $Fe/SiO_2/Si$, $Fe_3O_4/SiO_2/Si$ and $TiO_2/SiO_2/Si$ structures, which established the lateral photovoltage dependences on the thickness of the top layer, the type of substrate conductivity, and the photo-response of these structures under pulsed illumination.

Fig. 1 shows the dependences of the lateral photovoltage on the laser beam position at different thicknesses of the upper layer for the structures in which LPE has been observed: in the structure $Fe/SiO_2/Si$, LPE is observed on both types of conductivity substrates (Fig. 1, a and b), whereas in the case of Fe_3O_4 (Fig. 1, c) and TiO_2 (Fig. 1, d) films, LPE is only observed on n-Si and p-Si substrates, respectively. As can be seen in Figure 1, changing the type of conductivity of the substrate results in a change in the polarity of the LPE. In addition, for all structures, the sensitivity and non-linearity characteristics of the LPE depend on the thickness of the top layer.
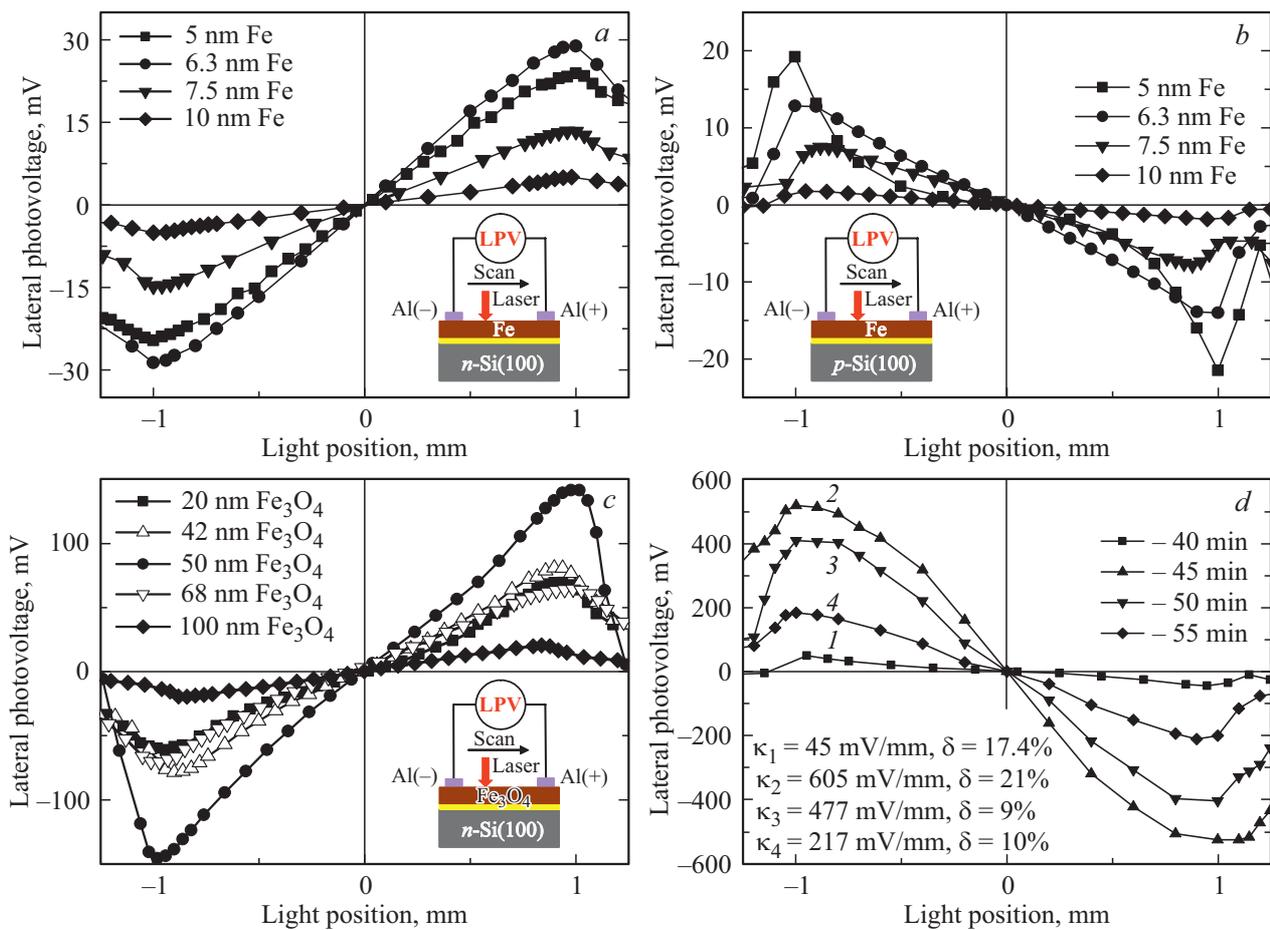
Figure 1. Dependencies of lateral photo-voltage on light spot position for structures (a) — Fe/SiO$_2$/n-Si; (b) — Fe/SiO$_2$/p-Si; (c) — Fe$_3$O$_4$/SiO$_2$/n-Si; (d) — TiO$_2$/SiO$_2$/p-Si.

Fig. 2 shows thickness dependences of LPE sensitivity and non-linearity for the investigated structures. As can be seen from Fig. 2, the thickness dependences of LPE sensitivity are extreme for all investigated structures, and LPE non-linearity dependences decrease exponentially with increasing thickness of the upper layer. From the analysis of Fig. 2, a it follows that the optimum thickness of iron films is ~ 6 nm and is independent of the substrate conductivity type, but the p-type substrate has lower sensitivity. At the same time, from comparing Fig. 2, a with Fig. 2, c and d, it follows that the thickness of the iron films is an order of magnitude smaller than for magnetite and TiO$_2$ films. This difference can be explained by the structural and morphological properties of the top layer films. From AFM and spectral ellipsometry data, it can be concluded that the iron film grows laterally as the lateral grain size of iron films is $15-25$ nm and exceeds the film thickness of 6.3 nm [24]. Unlike iron films, magnetite films, as shown in [25], exhibit columnar growth due to their predominant growth orientation perpendicular to the film plane, in which case the lateral grain size according to AFM is $25-35$ nm at an optimum film thickness of ~ 50 nm. The highest sensitivity in the case of TiO$_2$ film was observed at a

thickness of ~ 25 nm corresponding to 45 min deposition. In the work [23], it was shown that titanium dioxide films, as well as iron and magnetite films, have a polycrystalline structure. However, unlike structurally continuous iron and magnetite films, TiO$_2$ films are characterized by porosity.

From Fig. 2, b and c, it can be seen that for Fe/SiO$_2$/Si and Fe$_3$O$_4$/SiO$_2$/Si structures the non-linearity of LPE in the optimal thickness area is $5-6\%$, which is within the applicability for PSD. Significantly higher non-linearity values in the TiO$_2$/SiO$_2$/p-Si structure may be due to both the strong roughness and thus high scattering in this structure and electric field distortion in the near-contact region due to the high resistive layer TiO$_2$.

To explain the influence of the conductivity of the upper layer of the hybrid structure on the LPE, we calculated energy band diagrams of the investigated structures, which are shown in Fig. 3. It should be noted that these band diagrams have been constructed with the surface states at the SiO$_2$/Si interface in mind, since, as shown in [16,26,27], they are always present at the SiO$_2$/Si interface. These surface states pin the Fermi level, and lower the height of the built-in barrier [26,27]. Earlier we have shown [16,17] that ignoring the surface states leads to a mismatch between
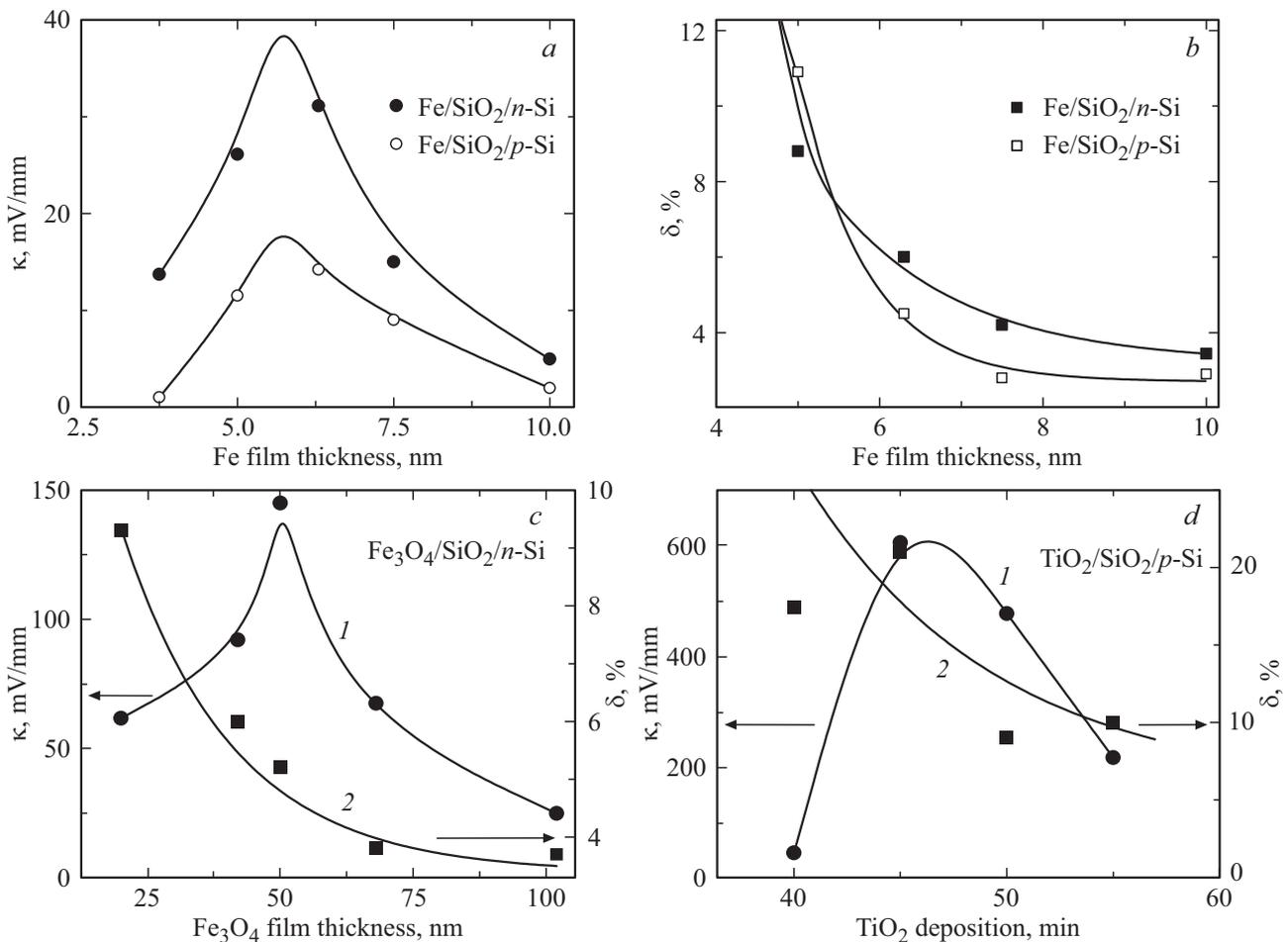
Figure 2. LPE sensitivity (a) and LPE non-linearity (b) thickness dependences for Fe/SiO$_2$/n-Si and Fe/SiO$_2$/p-Si structures; LPE sensitivity and non-linearity for structures Fe$_3$O$_4$/SiO$_2$/n-Si (c) and TiO$_2$/SiO$_2$/p-Si (d).

the experimental LPE results and the parameters of the idealized energy band diagrams.

By comparing Fig. 3, a and b, it can be seen that the direction of the built-in field at the SiO$_2$/Si interface changes as the type of conductivity of the silicon substrate changes. Accordingly, the direction of the built-in field determines the type of photo-generated carriers extracted to the SiO$_2$/Si interface, resulting in a reversal of the LPE polarity. In addition, depending on the material of the top layer, the magnitude of the built-in potential in the structures differs, which according to LPE theory is reflected in the magnitude of the lateral photovoltage.

The expression for the lateral photo-tension as a function of the position of the light spot, according to the theoretical model proposed in [5], is

$$LPV = K\left[\exp(\beta|\varphi_i|) - 1\right](|x_1| - |x_2|), \qquad (1)$$

where K — proportional coefficient depending on illumination intensity; $\beta = q/kT$ — temperature coefficient; φ_i — built-in potential; x_1, x_2 —distance from illumination point to measurement contacts. It follows from the above

expression that the LPV is exponentially dependent on the absolute value of the built-in potential.

According to the band diagrams in the Fe/SiO$_2$/n-Si structure shown in Figure 3, the built-in potential is 0.39 eV, and in the Fe/SiO$_2$/p-Si structure — 0.27 eV. Substituting these values into (1) shows that this difference in built-in potential is exactly what provides a 2.2 fold change in sensitivity. Moreover, from the comparison of the sensitivity value (Fig. 2, a) and the energy band diagrams (Fig. 3, a and b), it can be concluded that the maximum LPV values are achieved in MOS structures having an inversion layer at the SiO$_2$/Si interface (when $q\varphi_i > |E_F - E_i|$ [3]), since in this case, there is a sharper separation of electron-hole pairs at the quasi $p-n$-transition boundary.

In the Fe$_3$O$_4$/SiO$_2$/Si structure, the effect was observed only on silicon n-type substrate, since the large magnetite work function $q\varphi\text{Fe}_3\text{O}_4 = 5.2$ eV [28] leads to a high built-in potential $|q\varphi_i| = 0.58$ eV at the SiO$_2$/n-Si interface, whereas at the interface SiO$_2$/p-Si, the value of the built-in potential $|q\varphi_i| \sim 0.09$ eV. In this case, the SiO$_2$/n-Si interface forms an inversion layer, which, in turn, is the reason for the high value of LPE sensitivity equal to
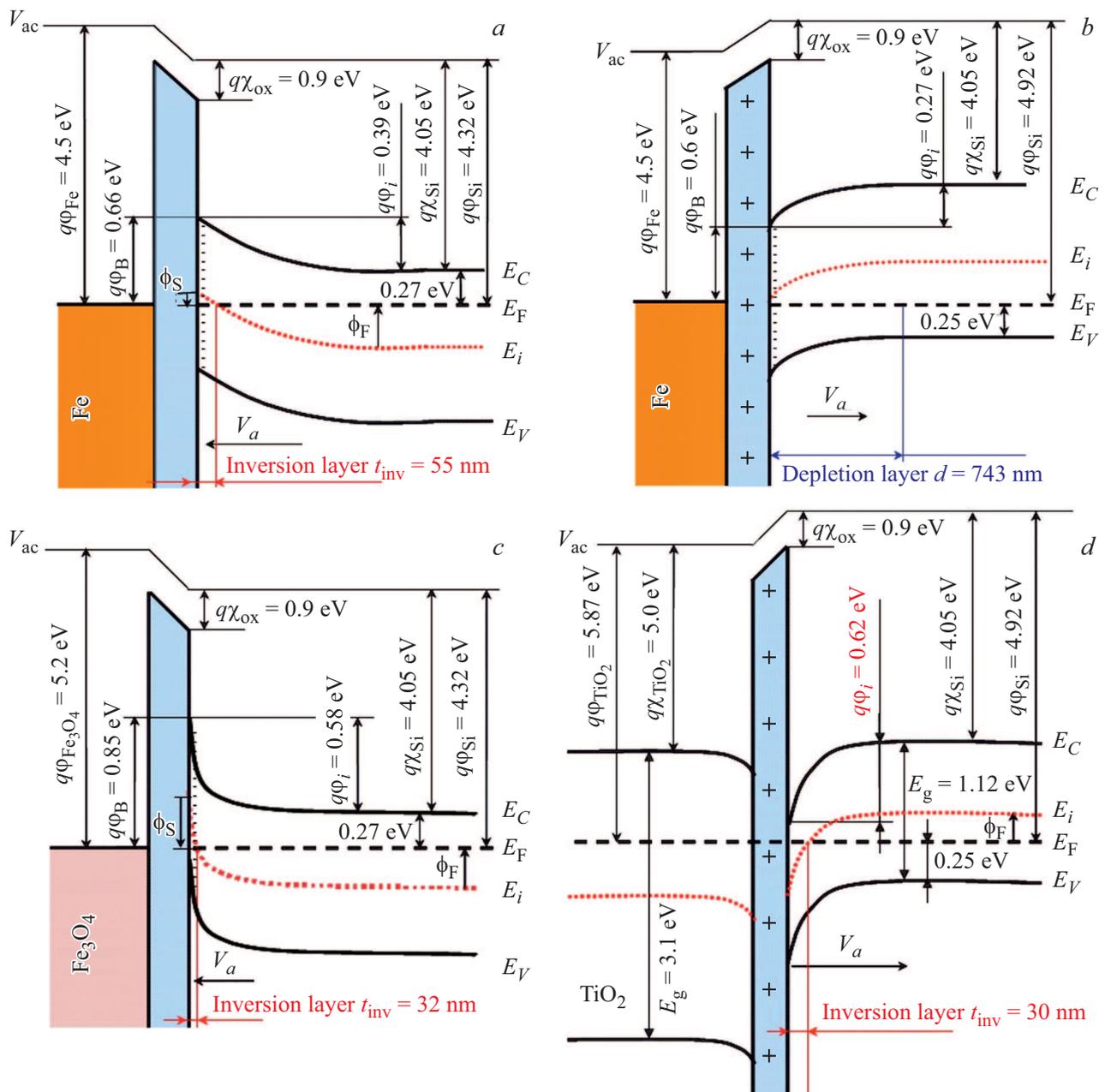
Figure 3. Energy band diagrams for hybrid structures: (*a*) — $Fe/SiO_2/n$-Si; (*b*) — $Fe/SiO_2/p$-Si; (*c*) — $Fe_3O_4/SiO_2/n$-Si; (*d*) — $TiO_2/SiO_2/p$-Si.

129 mV/mm, and in $Fe_3O_4/SiO_2/p$-Si structure according to above (1) a very weak photovoltage signal comparable to noise level is formed, and the photovoltage increase caused by contact phenomena [16] was observed near contacts.

Despite the even higher work function of titanium oxide $q\varphi_{TiO_2} = 5.87$ eV [29,30], no LPE is observed in the $TiO_2/SiO_2/n$-Si structure. The fact is that TiO_2 is a semi-isolator with a band gap width of 3.1 eV, and the energy band diagram is constructed for $n(-)n$ isotype heterostructure taking into account the surface states at the SiO_2/n-Si interface [31]. From the calculations given for

the $TiO_2/SiO_2/n$-Si structure, it was found that the built-in barrier height is only 0.16 eV and the LPV value is too small. At the same time, according to the energy band diagram for $TiO_2/SiO_2/p$-Si structure, taking into account the surface states of this $n(+)p$ structure, shown in Fig. 3, *d*, the built-in potential in it reaches a value of 0.62 eV, with an inversion layer forming at the SiO_2/p-Si interface.

As one would expect, according to theoretical calculations (1), in the $TiO_2/SiO_2/p$-Si structure the maximum LPE sensitivity increased to ~ 600 mV/mm, however, with a simultaneous increase in non-linearity to 21%. Based

on the performance requirements of the PSD [8,11], in this case, a sample with a sensitivity value of 477 mV/mm and non-linearity value of 9% should be chosen as the optimum thickness. The high values of LPE non-linearity in the $TiO_2/SiO_2/p$-Si structure are, in our opinion, due to lateral inhomogeneity of the integrated barrier and high resistivity in the contact area. The barrier heterogeneity can be attributed to the strong morphological roughness of the films. For example, it was shown in [32] that TiO_2, films deposited on a glass substrate for 1 hour, the roughness reaches $\sim$ 90 nm at a grain size of $\sim$ 150 nm.

Based on the above analysis of energy band diagrams, it can be concluded that hybrid structures whose energy band diagrams exhibit significant band bending at the SiO_2/Si interface in the turn-off type direction have high LPE sensitivity values. From the comparison of Fig. 3, a and b, it is seen that in the structure $Fe/SiO_2/Si$ when the Si substrate conductivity changes at the interface SiO_2/Si in both cases a depleted layer is formed, but the amount of band bending in these structures differs and the direction is opposite. As noted above, a higher value of LPE sensitivity is observed in the $Fe/SiO_2/n$-Si structure due to the stronger band bending at the SiO_2/Si interface. Whereas the opposite direction of the built-in field in these structures provides a polarity inversion of the lateral photovoltage.

The comparison of the energy band diagrams in Fig. 3, a and c shows that in both $Fe/SiO_2/n$-Si and $Fe_3O_4/SiO_2/n$-Si structures an inversion layer is formed at the SiO_2/n-Si interface. The difference between these diagrams is due to the magnitude of the Fe (metal) and Fe_3O_4 (semi-metal) work function, resulting in different band bending and hence lateral photovoltage.

Using TiO_2 as the top layer, the energy band diagram of $TiO_2/SiO_2/Si$ structure corresponds to the heterostructure (Fig. 3, d) in which an inversion layer is formed at the SiO_2/p-Si interface.

The theoretical calculations, based on the energy parameters of the energy band diagrams, constructed by us for the investigated structures allow us to state that the increase in the value of the built-in potential at the SiO_2/Si interface leads to an increase in the lateral photovoltage, and the change of the built-in field direction is accompanied by inversion of the polarity of the lateral photovoltage.

It should be noted that the extreme dependence of LPE sensitivity on the thickness of the upper layer has been observed earlier in works [9–18]. Generally, the nature of the change in thickness dependence of LPE sensitivity is explained from two perspectives. On the one hand, the reduction of LPE sensitivity in the low-thickness range is due to the disruption of film continuity and hence a reduction of the built-in field [33]. As the built-in field increases, the number of excess photo-carriers increases and diffusive scattering decreases, resulting in an increase in lateral photovoltage. The maximum LPE is reached when the film becomes continuous and the height of the built-in barrier — homogeneous [17,33]. On the other hand, the decrease in LPE sensitivity with increasing film
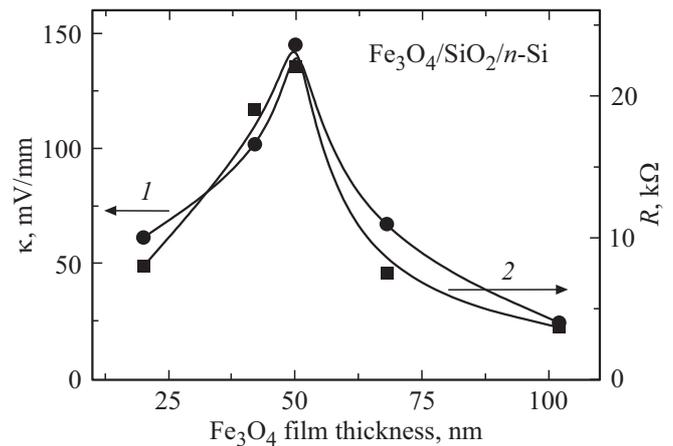
Figure 4. Thickness dependences of LPE sensitivity and resistance for $Fe_3O_4/SiO_2/n$-Si structure.

thickness after the maximum is attributed to a decrease in film resistance and the shorting of the two measuring electrodes.

To better understand the behavior of the LPE thickness dependence, we compared it to the thickness dependence of the resistivity (R) for the $Fe_3O_4/SiO_2/n$-Si structure measured between two contacts. As can be seen from Fig. 4, the character of the dependences coincides, which allows us to interpret the change in LPE sensitivity in terms of changes in the conductivity of the MOS structure. Earlier in work [34], it has been shown that in the area of room temperature in MOS structures with inversion layer and tunnel-thin silicon oxide with thickness of metal films up to 40 nm, it is impossible to measure the conductivity of the metal layer, because due to thermo-electronic emission the conductivity in them is determined by the ratio of conductivity of the upper metal layer and the inversion layer. In essence, a two-channel conductivity model with switching conductivity channels across the film and inversion layer has been proposed in the work [34]. Since the inversion layer has a higher conductivity at room temperature, most of the current is carried by the electron gas in the inversion layer. According to the authors [34], in the case of thicker metal films, their conductivity is higher than that of the inverted Si layer, resulting in conductivity predominantly through the film. This result indicates that switching of conductivity channels can be controlled not only by temperature but also by film thickness.

The two-channel model also applies to LPE, only now the photo-carriers can be injected from the inversion layer into the top layer as a result of thermal emission (Fig. 5). By analogy with the work [34] we can assume that at small film thicknesses, the resistance of the inversion layer (R_{inv}) in the near-surface area of the monocrystalline silicon substrate is much smaller than that of the polycrystalline film (R_{film}), and photocurrent flows through the inversion layer. However, until a homogeneous barrier is formed, the lateral current transfer does not take place through the inversion layer but rather through the spatial charge

Energy band structure and LPE characteristics data

Structure	E_g, eV	$q\varphi_i$, eV	t_{inv}, nm	R, kΩ (CVC)	κ, mV/mm	δ, %	U_{max}, mV	τ_R, μs	τ_F, μs
Fe/SiO$_2$/n-Si	0	0.39	57	1.8	31	6	29	3.93	3.85
Fe/SiO$_2$/p-Si	0	0.27		3.1	14	4.5	13	11	11
Fe$_3$O$_4$/SiO$_2$/n-Si	0.01	0.58	32	38	142	5.2	145	8	53
TiO$_2$/SiO$_2$/p-Si	3.1	0.62	30	92000	477	9.1	170	30	240
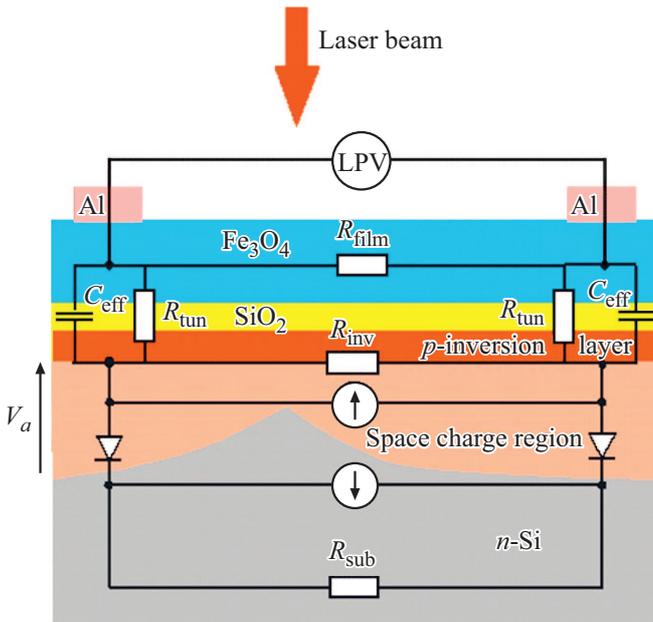
Figure 5. Equivalent circuit of two-channel lateral photoconductivity combined with Fe$_3$O$_4$/SiO$_2$/n-Si structure

area (SCA), which is orders of magnitude thicker than the inversion layer, which significantly reduces the conduction channel resistance across the near-surface layer of silicon. Thus, as a result of the heterogeneity of the barrier at low film thicknesses, the LPV has low values. As the film thickness and therefore the barrier homogeneity increases, there is an increase in the LPV. Once the barrier has reached homogeneity, the resistance of the inversion layer reaches saturation. As the film thickness increases, its resistance (R_{film}) decreases and when it becomes less than the resistance of the inversion layer (R_{inv}), the current is predominantly transferred through the film, which causes the two measuring electrodes to short out. It can be assumed that the LPE maximum in the thickness dependence is due to the switching of conduction channels across the inversion layer and the film, respectively, before and after the maximum in the thickness dependence, Fig. 4. It is likely that the maximum LPV is reached when the film conductivity is comparable to that of the inversion layer.

In the TiO$_2$/SiO$_2$/p-Si structure, the resistance of titanium oxide film is orders of magnitude higher than that of both iron and magnetite films, so the decrease of LPE

with increasing thickness of TiO$_2$ film after reaching the maximum is due, in our opinion, not by its resistance decrease, but by the contact voltage loss due to the high film resistance in the transverse direction (R_{tun}) (Fig. 5). The sensitivity remains very high compared to the results of [35,36], where TiO$_2$ films were obtained by magnetron reactive sputtering and had thicknesses in the range of $0.4-2.4$ nm. The sensitivity value for the Ti/0.16 nm$-$TiO$_2$/n-Si structure reached 169 mV/mm [35] and for the TiO$_2$/6.2 nm$-$Ti/n-Si$-$97 mV/mm [36]. The difference in sensitivity values in our experiment with the literature data is due to the way TiO$_2$ films are formed and their thickness.

As can be seen from the above analysis, the variation of LPE parameters in different structures is well explained by the energy band diagrams in terms of the presence of band bending in the near-surface area of silicon. Consequently, it can be assumed that the main mechanism of lateral photoconductivity will be through the inversion layer adjacent to the SiO$_2$/Si interface, while the top layer serves only to create an built-in barrier at the SiO$_2$/Si interface.

The optical response and LPE relaxation time are also important characteristics for PSD. Therefore, we investigated the time dependence of the lateral photo-voltage under localised pulsed illumination in the near-contact area. Laser pulse time profiles at room temperature for Fe/SiO$_2$/n-Si, Fe$_3$O$_4$/SiO$_2$/n-Si and TiO$_2$/SiO$_2$/p-Si structures are shown in Figure 6. As can be seen from Fig. 6, a, an increase in the resistivity of the upper layer results in both an increase in the photovoltage signal and a change in the shape of the photo-response signal. For comparison, the energy band structure and LPE characteristics, including photo-response times, are given in the table.

The table shows that in MOS structures, the pulse amplitude U_{max} of the photo-response corresponds to the LPE sensitivity, while in the heterostructure the amplitude $U(t)$ is almost 3 fold less than the LPE sensitivity (κ). In our opinion, in all the investigated structures the amplitude of $U(t)$ is initially determined by the value of the built-in potential, however, in the case of a heterostructure, there is a voltage loss in the transverse direction of the structure in the contact area. On the other hand, the rise τ_R and fall time τ_F in Fe$_3$O$_4$/SiO$_2$/n-Si and TiO$_2$/SiO$_2$/p-S structures is related to the increase of system resistance R measured between the two contacts.

From the comparison of the photo-response signals in Fig. 6 it can be seen that in the Fe/SiO$_2$/n-Si structure the
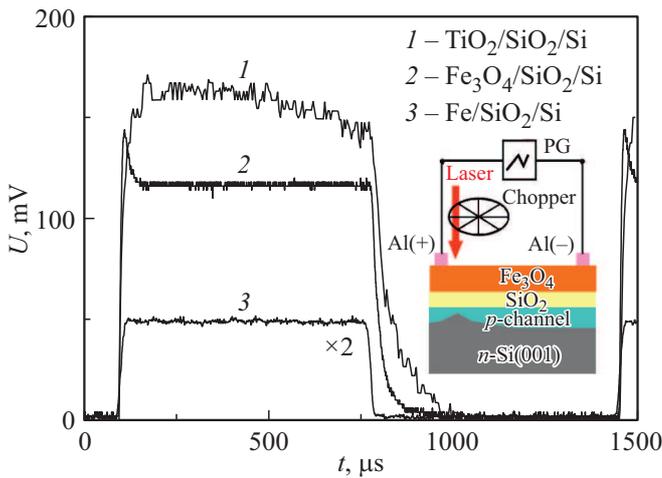
Figure 6. Time dependences of lateral photovoltage in structures $TiO_2/SiO_2/p$-Si, $Fe_3O_4/SiO_2/n$-Si and $Fe/SiO_2/n$-Si. The inset shows a schematic illustration of an experiment to study the temporal response of structures under pulsed illumination with a period of $T = 1.36$ ms and a pulse duration of $1/2T$.

rise and fall time constants are the same — the signal has an almost rectangular shape, Whereas in $Fe_3O_4/SiO_2/n$-Si and $TiO_2/SiO_2/p$-Si structures, the rising and falling edges of photovoltage signal are asymmetrical, with the falling time in these structures much longer than the rising time. In the present work, the rise time is defined as the time required to increase the photovoltage from 10% to 90% of the photovoltage peak (U_{max}), and the fall time is defined as the time required to decrease the photovoltage from 90% to 10% U_{max} [37]. In the open circuit measurement, the rise time of $Fe_3O_4/SiO_2/n$-Si structure is 8.5 times higher than that of $Fe/SiO_2/n$-Si structure, where it is $3.9\,\mu$s, and ~ 7.6 times shorter than the rise time in the structure $TiO_2/SiO_2/p$-Si. Significantly larger differences are observed for decay time. From analysis of the decaying fronts of the photovoltage signal, the decay time is 3.8, 53 and $240\,\mu$s in $Fe/SiO_2/n$-Si, $Fe_3O_4/SiO_2/n$-Si and $TiO_2/SiO_2/p$-Si structures, respectively.

On the other hand, the characteristics of the photoresponse are often the rise and fall time constants, which are derived from approximations of the rise and fall processes. In our case, the rise time constants are determined by fitting the ramp-up process using a Boltzmann sigmoidal function

$$U(t) = U_2 + \frac{U_1 - U_2}{1 + \exp\big((t - t_s)/\tau_R\big)},$$

where U_1 — the initial photovoltage value, U_2 — the final photovoltage value, t_S —the time center, and τ_R — the time constant for the ramp-up process. The rise time constants (τ_R), represented by the sigmoidal Boltzmann approximation, at room temperature in the open measurement scheme are 4.2 ± 0.1, 2.26 ± 0.06 and $5.2 \pm 0.6\,\mu$s for $Fe/SiO_2/n$-Si, $Fe_3O_4/SiO_2/n$-Si and $TiO_2/SiO_2/p$-Si, structures, respectively. However, the high error of the time

parameter in the structure $TiO_2/SiO_2/p$-Si indicates that in this case it is better to use exponential approximation, which determines the value of the ramp-up time constant $16 \pm 1\,\mu$s.

For the $Fe/SiO_2/n$-Si structure, the damping curves as well as the rise curves corresponded to a Boltzmann sigmoidal function and the relaxation time constant in the open measurement scheme is $3.7 \pm 0.2\,\mu$s. With increasing resistivity of the upper layer material in hybrid structures, the fitting parameters for the decay time constant are different. For the $Fe_3O_4/SiO_2/n$-Si structure, the relaxation time constant has been determined using a simple exponential function and is $\sim 23\,\mu$s in an open measurement scheme. Whereas for the structure $TiO_2/SiO_2/p$-Si, a biexponential function with relaxation time constants of 25 and $125\,\mu$s was required to approximate the relaxation time. In addition, in the case of the $Fe_3O_4/SiO_2/n$-Si structure, a peak is observed on the rising front when the light is turned on. The relaxation time constant at the peak has been determined using a simple exponential function and is $\sim 15\,\mu$s.

This difference in the behavior of the structures under pulsed illumination can be explained using an equivalent diagram (Fig. 7). As a first approximation of an equivalent electrical circuit for our structures, we have accumulated the equivalent circuits previously presented for the photocell [38] and the lateral photoelectric effect [19,20]. As a result, our equivalent circuit (Fig. 7) contains the following elements: C_{pn} and R_{pn} — capacitance and resistance in the non-equilibrium photocarrier separation area near the SiO_2/Si interface, characterizing the photocarrier generation process, R_{inv} and R_{film1} — longitudinal resistances of the inversion layer and magnetite film, characterizing the lateral diffusion of photo-carriers, as well as capacitances and resistances arising in hybrid structures in the aluminum contact area: C_{ss}, C_{dep}, C_{ox} — capacitance of surface states, spatial charge area, silicon oxide layer, R_{ss} — resistance of surface states [39]. For DC and AC operation of the circuit, we have introduced $R_{tun} = R_{dep} + R_{SiO_2} + R_{film,t}$ tunnel resistance in the contact area in the transverse direction to the surface.

In a detailed analysis of the hybrid structures under study, three variants of the equivalent scheme can be proposed for the three types of conductivity of the upper layer: i — metal, ii — semi-metal and iii — semi-insulator.

i — In the case of MOS structures with a metallic top layer, the transient characteristics will only be determined by the RC-filter consisting of the distributed characteristics of the silicon surface and the silicon oxide layer (no additional RC-filter for the film).

ii — In the case of MOS structures with a semi-metallic top layer, to the substrate surface layer filter, only the film resistance in the transverse direction (only the active resistance ($R_{film,t}$) from the additional RC-filter is included in the circuit) is added in series.

iii — Whereas in the case of a heterostructure, an additional RC-filter of the substrate surface layer (the additional
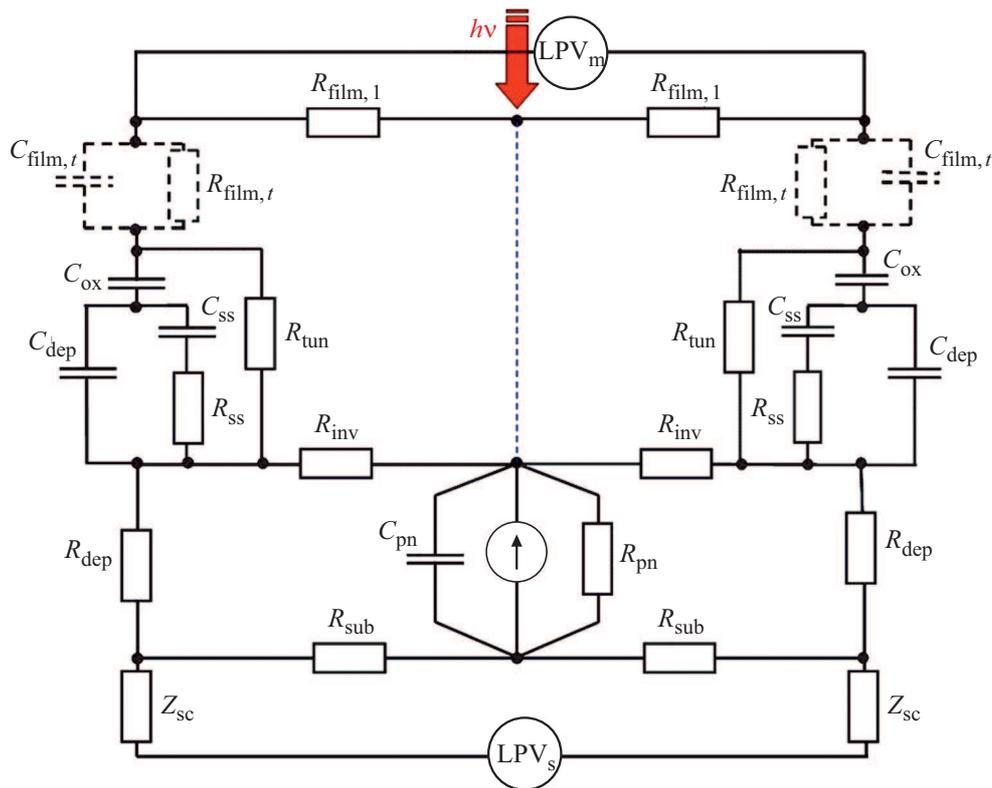
Figure 7. Equivalent circuit of lateral photoconductivity under pulsed illumination. The lower part characterizes the conductivity of the photo-separated carriers on the substrate side.

RC-filter accounts for the impedance characteristics ($C_{\text{film},t}$ and $R_{\text{film},t}$) of the TiO$_2$ film) is added to the RC-filter.

The considered equivalent circuits reflect the two-channel mechanism of lateral photoconductivity. Such a significant difference in timing in hybrid structures with different conductivity of the top layer is due to the RC-characteristics of the circuit in the measuring contact area. The symmetric photovoltage waveform in the Fe/SiO$_2$/n-Si structure is realized when there is no contribution from the top layer to the transient response. The peak presence on the rising front in the case of the Fe$_3$O$_4$/SiO$_2$/n-Si structure indicates that the electron density in the illuminated area of the photoconductor reaches the amplitude area before the electric field has completely weakened in that area. The delay of photo-response process in Fe$_3$O$_4$/SiO$_2$/n-Si and TiO$_2$/SiO$_2$/p-Si structures is due to the change of RC-characteristics of the electrical contact due to the contribution of impedance properties of the top layer to contact phenomena.

Thus, the transient LPE in hybrid structures can be adequately interpreted by an equivalent RC-chain scheme that changes configuration when the conductivity of the top layer changes. This scheme is a generalization of the two-channel model of lateral photoconductivity to both the case of continuous and pulsed illumination. The fact that in heterostructures the upper semi-insulator layer is not involved in the photo-conversion of photo-generated carriers supports the traditional view that LPE is a semiconductor effect, and not only the generation and separation of electron-hole pairs but also the current transfer (with recombination processes along $p-n$-transition) takes place in the near-surface silicon layer. In MOS structures, the metallic layer does shunt the conduction channel across the inversion layer, but not as a conduction channel (in resulting separation) of photo-generated carriers, but only as a load resistance. It is important to note that the role of contact phenomena in the simplified measuring circuit [13] has not previously been taken into account in the LPE study, which makes understanding the mechanism of lateral current transfer very difficult.

4. Conclusion

A study of the effect of top layer material conductivity on LPE in SiO$_2$/Sibased hybrid structures has shown that the dependences of LPE sensitivity on film thickness for all types of structures are extreme, and the choice of top layer material influences the range of optimal thicknesses. It is found that the value of lateral photovoltage in hybrid structures is determined by the value of the built-in potential at the SiO$_2$/Si interface, depending on the work funcyion of the upper layer material, rather than a decrease in its conductivity. It is suggested that the increase in non-linearity in the system TiO$_2$/SiO$_2$/p-Si is related to the morphological properties of titanium dioxide films. It is shown that the

temporal characteristics of LPE under pulsed illumination are due to the impedance characteristics of the *RC*-chain in the near-contact areas. The results allowed us to identify the mechanism of lateral photoconductivity: the lateral current transfer takes place via diffusion-recombination processes of photo-separated excess carriers across the inversion layer and silicon bulk, while the top layer serves only to form a quasi $p-n$-transition at the SiO_2/Si interface. The sensitivity and non-linearity LPE parameters, as well as the transient LPE characteristics of the studied hybrid structures, make them promising candidates for high-performance position-sensitive detectors. The structures of greatest interest are those with a semi-metallic top layer.

Financial support of work

Conflict of interest

The authors declare that they have no conflict of interest.

References

[1] J.T. Wallmark. Proc. IRE **45**, *4*, 474 (1957).

[2] G. Lucovsky. J. Appl. Phys. **31**, *6*, 1088 (1960).

[3] S.M. Sze, K.K. Ng. Physics of semiconductor devices. John Wiley & Sons, N.Y. (2006). P. 832.

[4] T. Shikama, H. Niu, M. Takai. Jpn.. J. Appl. Phys. **23**, *10R*, 1314 (1984).

[5] P.P. Konorov, Yu.A. Tarantov. V sb.: LSU Academic Notes. Ser. fiz. **370**, *17*, 114 (1974).

[6] E. Fortunato, G. Lavareda, R. Martins, F. Soares, L. Fernandes. Sens. Actuat. A **51**, 135 (1996).

[7] D.J.W. Noorlag. Lateral-photoeffect position-sensitive detectors. Ph.D. Thesis. Delft University of Technology, Delft, The Netherlands (1982). P. 211.

[8] J. Henry, J. Livingstone. J. Phys. D **41**, *16*, 165106 (2008).

[9] S.Q. Xiao, H. Wang, C.Q. Yu, Y.X. Xia, J.J. Lu, Q.Y. Jin, Z.H. Wang. New J. Phys. **10**, *3*, 033018 (2008).

[10] H. Wang, S.Q. Xiao, C.Q. Yu, Y.X. Xia, Q.Y. Jin, Z.H. Wang. New J. Phys. **10**, *9*, 093006 (2008).

[11] C. Yu, H. Wang. Sensors **10**, *11*, 10155 (2010).

[12] L.Z. Hao, Y.J. Liu, Z.D. Han, Z.J. Xu, J. Zhu. J. Alloys Compd. **735**, 88 (2018).

[13] S. Qiao, B. Liang, J. Liu, G. Fu, S. Wang. J. Phys. D **54**, 153003 (2021).

[14] X. Wang, B. Song, M. Huo, Y. Song, Z. Lv, Y. Zhang, Y. Wang, Y. Song, J. Wen, Y. Sui, J. Tang. RSC Advances **5**, *80*, 65048 (2015).

[15] B. Song, X. Wang, B. Li, L. Zhang, Z. Lv, Y. Zhang, Y. Wang, J. Tang, P. Xu, B. Li, Y. Yang, Y. Sui, B. Song. Opt. Exp. **24**, *21*, 23755 (2016).

[16] T.A. Pisarenko, V.V. Balashev, V.A. Vikulov, A.A. Dmitriev, V.V. Korobtsov. FTT **60**, *7*, 1311 (2018) (in Russian).

[17] T.A. Pisarenko, V.V. Balashev, V.V. Korobtsov, A.A. Dimitriev, V.A. Vikulov. Defect Diffusion Forum **386**, 137 (2018).

[18] X. Wang, X. Zhao, C. Hu, Y. Zhang, B. Song, L. Zhang, W. Liu, Z. Lv, Y. Zhang, J. Tang, Y. Sui, B. Song. Appl. Phys. Lett. **109**, *2*, 023502 (2016).

[19] A.K. Dutta, Y. Hatanaka. Solid-State Electron. **32**, *6*, 485 (1989).

[20] C. Narayanan, A.B. Buckman, I. Busch-Vishniac, W. Wang. IEEE Transact. Electron Devices **40**, *9*, 1688 (1993).

[21] G. Prestopino, M. Marinelli, E. Mitani, C. Verona, G. Verona-Rinati. Appl. Phys. Lett. **111**, *14*, 143504 (2017).

[22] H. Kobayashi, Asuha, O. Maida, M. Takahashi, H. Iwasa. J. Appl. Phys. **94**, *11*, 7328 (2003).

[23] D.P. Opra, S.V. Gnedenkov, S.L. Sinebryukhov, A.B. Podgorbunsky, A.A. Sokolov, A.Yu. Ustinov, V.G. Kuryavy, V.Yu. Mayorov, V.V. Zheleznov. Electrochemical Energy **19**, *3*, 123 (2019).

[24] V.V. Balashev, V.V. Korobtsov. ZhTF **88**, *1*, 75 (2018). (in Russian)

[25] V.V. Balashev, V.V. Korobtsov, T.A. Pisarenko, L.A. Chebotkevich. ZhTF **81**, *10*, 122 (2011) (in Russian)

[26] A.M. Cowley, S.M. Sze. J. Appl. Phys. **36**, *10*, 3212 (1965).

[27] S. Ghosh, P.C. Srivastava. J. Electron. Mater. **43**, *11*, 4357 (2014).

[28] M. Fonin, R. Pentcheva, Yu.S. Dedkov, M. Sperlich, D.V. Vyalikh, M. Scheffler, U. Rüdiger, G. Güntherodt. Phys. Rev. B **72**, 104436 (2005).

[29] Z. Zhao, Z. Li, Z. Zou. J. Phys.: Condens. Matter **22**, *17*, 175008 (2010).

[30] A. Kiejna, T. Pabisiak, S.W. Gao. J. Phys.: Condens. Matter **18**, *17*, 4207 (2006).

[31] B.L. Sharma, R.K. Purohit. Semiconductor heterojunctions. Pergamon Press, Oxford (1974). P. 224.

[32] J. Lias, S.A. Shahadan, M.S.A. Rahim, N. Nayan, M.K. Ahmad, M.Z. Sahdan. J.Teknologi. **78**, *10*, 1 (2016).

[33] X. Huang, C. Mei, J. Hu, D. Zheng, Z. Gan, P. Zhou, H. Wang. IEEE Electron Device Lett. **37**, *8*, 1018 (2016).

[34] J. Dai, L. Spinu, K.Y. Wang, L. Malkinski, J. Tang. J. Phys. D **33**, *11*, L65 (2000).

[35] S. Liu, C.Q. Yu, H. Wang. IEEE Electron Device Lett. **33**, *3*, 414 (2012).

[36] C.Q. Yu, H. Wang, Y.X. Xia. Appl. Phys. Lett. **95**, *26*, 263506 (2009).

[37] W.S. Levine. The control handbook. Jaico Publishing House, Mumbai (1999).V. 1. P. 158.

[38] K. Lehovec, A. Slobodskoy. Solid-State Electron. **7**, *1*, 59 (1964).

[39] T.A. Pisarenko, V.V. Korobtsov, V.V. Balashev, A.A. Dimitriev. Solid State Phenomena **312**, 92 (2020).